

DR. CONCHA ARENAS (Orcid ID : 0000-0002-4212-0524)

Article type : Original Manuscript

Corresponding author mail id: carenas@unizar.es

Seasonal temperatures from $\delta^{18}\text{O}$ in Recent Spanish tufa stromatolites: Equilibrium redux!

C. ARENAS*, C. OSÁCAR*, L. AUQUÉ*, J.E. ANDREWS†, G. PARDO*, A. MARCA†,
L. MARTÍN-BELLO*, F.J. PÉREZ-RIVARÉS*

*Department of Earth Sciences, University of Zaragoza, 50009 Zaragoza (Spain)

†School of Environmental Sciences, University of East Anglia, Norwich, NR4 7TJ (United Kingdom)

Associate Editor – Alexander Brasier

Short Title – Temperatures in Recent Spanish tufa stromatolites

ABSTRACT

This study focuses on recent debate over the value of stable isotope based environmental proxies recorded in riverine tufa-stromatolites. A twelve-year record (1999 to 2012) of river-bed tufa stromatolites in the River Piedra (north-east Spain) was recovered in this study, along with a partly overlapping fifteen-year record (1994 to 2009) of accumulations in a drainage pipe: both deposits formed in water with near identical physico/chemical parameters. Measured water temperature data and near constant $\delta^{18}\text{O}_{\text{water}}$ composition allowed selection of an ‘equilibrium’ palaeotemperature equation that best replicated actual temperatures. This study, as have previous studies, found that both

This article has been accepted for publication and undergone full peer review but has not been through the copyediting, typesetting, pagination and proofreading process, which may lead to differences between this version and the Version of Record. Please cite this article as doi: 10.1111/sed.12440

This article is protected by copyright. All rights reserved.

the Epstein et al. (1951) and Kim & O'Neil (1997) formulas for water temperature calculation from equilibrium calcite $\delta^{18}\text{O}$ compositions were appropriate for the River Piedra where tufa deposition rates are high, with means between 5.6 mm and 10.8 mm in six months. The $\delta^{18}\text{O}_{\text{calcite}}$ in both the river and the pipe deposits essentially records the full actual seasonal water temperature range. Only the coldest times (water temperature $<10^\circ\text{C}$), when calcite precipitation mass decreased to minimum, are likely to be unrepresented, an effect most noticeable in the pipe where depositional masses are smaller and below sample resolution. While kinetic effects on $\delta^{18}\text{O}_{\text{calcite}}$ -based calculated water temperature cannot be ruled out, the good fit between measured water temperature and $\delta^{18}\text{O}_{\text{calcite}}$ -calculated water temperature indicates that temperature is the principal control. Textural and deposition rate variability between the river and pipe settings are caused by differences in flow velocity and illumination. In the river, calcification of growing cyanobacterial mat occurred throughout the year, producing composite dense and porous laminae, whereas in the pipe, discontinuous cyanobacterial growth in winter promoted more abiogenic calcification. High-resolution $\delta^{18}\text{O}_{\text{calcite}}$ data from synchronous pipe and river laminae show that reversals in water temperature occur within laminae, not at lamina boundaries, a pattern consistent with progressive increase in calcite precipitation rate as cyanobacterial growth re-established in spring.

Keywords: Palaeotemperature equation, recent tufa stromatolites, seasonal pattern, stable isotopes, textural and deposition rate variability.

INTRODUCTION

Carbonates that precipitate in springs, rivers and lake shorelines in association with biotic substrates and under ambient water temperatures are known collectively as tufas. The concept that these deposits offer an attractive complementary climate archive to speleothems is well-established (e.g. Andrews & Brasier 2005; Andrews 2006). Tufa stromatolites are both spatially abundant and often have seasonal laminae that allow resolution of temperature variability (Matsuoka et al., 2001; Brasier et al., 2010)

through oxygen isotope compositions. Unlike most speleothems, which typically form sub-millimetre scale annual growth layers (e.g. Fairchild et al., 2006), tufa stromatolites can precipitate calcite rapidly and some active laminar tufas preserve intra annual geochemical signals (Matsuoka et al., 2001; Kano et al., 2007; Osácar et al., 2013, 2016). While this rapid tufa calcite precipitation has the advantage of building thick laminae, suitable for even sub-seasonal-scale sampling, it brings with it the spectre of oxygen isotopic disequilibrium effects caused by the precipitation kinetics (Yan et al., 2012; Sun et al., 2014; Wang et al., 2014; Kele et al., 2015; Zavadlav et al., 2016).

Historically, the earlier tufa stable isotope studies (for a review, see Andrews, 2006) focused on *relative* temperature reconstruction and broadly used the equilibrium relationships of Epstein et al. (1951), Epstein & Mayeda (1953) and the modifications by Craig (1965) to interpret the data. Lately, however, the experimental Kim & O'Neil (1997) equation has been widely used in more precise attempts at palaeotemperature reconstructions, notably in slow-growing speleothems, where its relationship to true equilibrium has recently been questioned (e.g. Coplen, 2007; Dietzel et al., 2009; Tremaine et al., 2011; Day & Henderson, 2011; Affek & Zaarur, 2014; Kele et al., 2015). Looking forward, it might soon be possible to use a clumped isotope approach to help address these issues (e.g. Kele et al., 2015) but right now preliminary unpublished clumped isotope data (from authors of this paper) for European ambient temperature tufas is not straightforward to interpret; neither is the sample mass currently required suitable for high resolution sampling.

In the context of this equilibrium/disequilibrium debate, tufa stromatolites may be instructive, because recent high quality field data (e.g. Osácar et al., 2013, 2016; Sun et al., 2014; Zavadlav et al., 2016) suggests that the 'equilibrium' relationship of Kim & O'Neil (1997), or the very similar equation by Epstein et al (1951), may well be appropriate for fast-depositing tufas, whereas slower growing tufa calcites may be better described by the Coplen (2007) equilibrium relationship (e.g. Yan et al., 2012) consistent with results from some speleothems (Tremaine et al., 2011; Kele et al., 2015).

This paper describes an active system where tufa stromatolites have formed both in a natural river setting and in a drainage pipe that diverted water from the river. The system has excellent temperature records affording the opportunity to select an equation that best replicates actual temperatures. This enables both textural and stable isotopic data to be decoded, in terms of actual temperatures, and make direct comparison between the pipe record and the river record, an important step as some workers claim that tufa stromatolites in recent drainage pipes (and open stream conditions) have questionable value as environmental indicators (Lojen et al., 2004, 2009; Zavadlav et al., 2016).

STUDY SITE: GEOLOGICAL SETTING, CLIMATE, HYDROLOGY AND SEDIMENTOLOGICAL CONTEXT

The River Piedra is a north flowing indirect tributary of the River Ebro in the the Iberian Range (Fig. 1A and B). This karst river, flowing on Mesozoic carbonate bedrocks, has extensive Quaternary fluvial tufa deposits (Sancho et al., 2015) and active tufa formation. Periodic monitoring of hydrochemical, sedimentological and geochemical parameters from 1999 to 2012 provides a time series of data that allows six-month correlation between sediment attributes and environmental parameters, including hydrophysics, hydrochemistry, air temperature and precipitation (Arenas et al., 2014).

The regional climate is continental Mediterranean with strong seasonal contrasts in temperature and precipitation. From October 1999 to September 2012, mean monthly air temperature varied between highs of 21.7 to 25.0°C (in July and August) and lows of 2.4 to 7.0°C (between December and February). The mean annual rainfall was 397 mm, with maxima in April, May and October (air temperature and precipitation data provided by *Agencia Estatal de Meteorología*; values averaged from the La Tranquera and Milmarcos meteorological stations, *ca* 700 m and 1050 m above sea level, respectively). Using these data, the spring and summer (March 21 to September 22) is assigned as the ‘warm’ period, and autumn and winter (September 22 to March 21) as the ‘cool’ period. Water temperature variation in the River Piedra shows a mean difference of 6°C between winter (mean of

10.5°C) and summer (mean of 16.5°C), and of 4.6°C between the warm and cool periods (based on hourly measurement data from June 2007 to September 2012).

The River Piedra is fed by base flow from an aquifer hosted in Middle Jurassic and Upper Cretaceous carbonate rocks. The main natural springs, near Cimballa (Fig. 1B), have a mean historical discharge of 1.4 m³/sec. From October 1999 to September 2012, the mean annual discharge was *ca* 1.06 m³/sec (data from Confederación Hidrográfica del Ebro, <http://195.55.247.237/saihebro/>). Maximum discharges occur in winter and minima in summer, but the river did not dry out during observations over the last 20 years.

The river water is of HCO₃-SO₄-Ca type, with mean pH = 8.03 and mean saturation index with respect to calcite (SIc) = +0.73 (measured biannually from 1999 to 2012 at 20 sites; Arenas et al., 2014). Table 1 shows values at sites P-14 and P-16 in the Monasterio de Piedra Natural Park (see Fig. 1C for location). Calcite (tufa) precipitation is first observed approximately 8 km downstream of the main springs (Vázquez-Urbez et al., 2010; Arenas et al., 2014).

Sedimentological context

The fluvial tufa deposits form in a wide array of sub-environments and related facies (Arenas et al., 2014). In the Monasterio de Piedra Natural Park, tufa stromatolites develop mainly in: (i) fast flowing water (>80 cm/sec) associated with inclined slopes, devoid of macrophytes; and (ii) stepped waterfalls (1 to 10 m high) where water flow can be slow or rapid. In these latter settings, tufa stromatolites form in faster-flowing zones, but are associated with non-laminated, calcite-coated moss and filamentous-algal deposits that form in lower flow areas.

River Piedra tufa deposition rates (1999 to 2012) are dependent on flow conditions (Arenas et al., 2014). Higher rates (mean = 14.0 mm/year) are found in the fast-flowing conditions where tufa stromatolites form, while stepped waterfalls have lower rates (mean = 7.8 mm/year). Moreover, tufa stromatolite deposition is thicker in warm periods (mean six-month deposition rates of 10.5 mm in warm periods and 5.3 mm in cool periods), reflecting temperature-dependent parameters, i.e. calcite

and CO₂ solubility in water and development of flora and prokaryotes and concomitant photosynthetic CO₂ uptake. Tufa stromatolites thus preserve the most continuous sedimentary record when compared to other facies (Arenas et al., 2014).

MATERIALS AND METHODS

This study focuses on a reach of the River Piedra approximately between sites P-14 and P-16 (Fig. 1C). Here the bed has a mean slope of 7° over *ca* 100 m, with decimetre high steps. Extensive tufa stromatolites form in the rapids and steeper zones, which typically are devoid of macrophytes (Fig. 2A and B). Water velocity at these zones varied between 1.3 m and 2.2 m/sec and water depth between 6.0 cm and 9.0 cm. At sites P-14 and P-16 (Fig. 1C) tablets were installed to collect a tufa deposit record from November 1999 to September 2012. Mean deposition rates at these sites were 16.0 mm/year in P-14 and 16.5 mm/year in P-16 (Arenas et al., 2014).

Twenty metres upstream of site P-14 some water was diverted by an artificial drainage pipe (8 m long, 25 cm in diameter, 3 to 5° inclination) buried at least 20 cm below a path and shaded from direct insolation (Fig. 1C). Water flow in the pipe was not regulated artificially, but flow was continuous with depth varying from 6 or 7 cm to 18 cm and water velocity from 2 to 2.3 m/sec. The pipe was removed in the spring of 2009, and a calcite deposit retrieved for comparison with the river sites (Fig. 3).

Field measurements

Water depths and velocities were measured at the river stations and in the pipe. Velocity was measured with a Water Flow Probe (Model FP101, Global Water, Gold River, CA, USA) at the entrance and exit of the pipe, and also by measuring float travel time through the pipe (March and September 2009). River station velocity was measured at the end of each season from 1999 to 2012 (Table 1).

Water temperature (T_w) in the pipe was assumed to be the same as T_w measured at the closest two river sites; the pipe being buried below ground, shaded and with continuous rapid through-flow. Water temperature was measured at the end of December and beginning of January (middle of the cool period) and at the end of June (middle of the warm period), from 1999 to 2012, at each tablet site. A continuous hourly record of T_w was also obtained from two data loggers (HOBO Pro V2; Onset, Cape Cod, MA, USA) installed at river sites 8 and 20 (Fig. 1C) from June 2007 to September 2012 (Table 1).

Hydrogeochemical and water $\delta^{18}\text{O}$ data ($\delta^{18}\text{O}_{\text{water}}$) measured between 2000 and 2012 from eight sites (end December or beginning January for the cool period and end of June for the warm period) are available in Arenas et al. (2014) and Osácar et al. (2013, 2016).

Sediment for stable isotope analyses

Tablets P-14 and P-16 (25 x 15 x 2 cm) were recovered twice a year (end of summer and end of winter) for six-month thickness measurement and sampling (see details in Vázquez-Urbez et al., 2010). A total of 26 consecutive six-month deposits were sub-sampled for stable isotope analyses with a micro-drill, with up to three samples from each six-month deposit collected (data in Osácar et al., 2016) and hereafter named ‘bulk’ samples. The mean values are included in Supporting Information. In most cases one ‘bulk’ sample per lamina was also microdrilled from section ‘Tbx’ of the pipe deposit (Fig. 3A), while in thicker laminae up to three samples were taken. A total of 31 consecutive laminae were sampled and the results are included in Supporting Information.

To explore precise relationships between the pipe and river deposits, and to understand potential for aliasing in the bulk data, temporally overlapping high-resolution sampling (HRS) was done by serial milling using a hand held micro-file. In the pipe deposit 72 samples were recovered from laminae 28 to 31 (see below Fig. 6A) and in river tablet P-14, 64 samples were recovered from 5.5 cm of deposit representing warm 2008, cool 2008/2009 and warm 2009 deposition (Fig. 2C). Mean

thickness of the milled samples was 850 μm (tablet) and 120 μm (pipe deposit); the data are included in the Supporting Information.

Stable isotope measurements were performed at the Serveis científico-tècnics of the University of Barcelona (UB, Spain), following classical protocols (McCrea, 1950). CO_2 produced by carbonate dissolution with 100% PO_4H_3 over 3 minutes at 70°C was analysed in a Thermo Finnigan MAT-252 spectrometer (Thermo Fisher Scientific, Waltham, MA, USA). The HRS and isotopic analyses (University of East Anglia Stable Isotope Laboratory, UEA) were made on $75 \pm 5 \mu\text{g}$ samples, reacted with 105% ($\rho = 1.92 \text{ gml}^{-3}$) phosphoric acid (H_3PO_4) at 90°C in an on-line common acid bath. The evolved CO_2 was purified and analysed for $\delta^{18}\text{O}$ and $\delta^{13}\text{C}$ using a Europa SIRA II dual inlet isotope ratio mass spectrometer (Europa Scientific Ltd., Crewe, UK). The data are calibrated to international reference scales Vienna Pee-Dee Belemnite (VPDB) and Vienna Standard Mean Ocean Water (VSMOW) using IAEA certified reference material NBS-19. Repeat analysis of both international and internal reference materials gave 1σ errors of 0.02‰ for $\delta^{13}\text{C}$ and 0.03‰ for $\delta^{18}\text{O}$ (UB) and 0.07‰ for $\delta^{13}\text{C}$ and 0.09‰ for $\delta^{18}\text{O}$ (UEA).

Water temperature calculation

The water temperatures (T_w) calculated from calcite $\delta^{18}\text{O}$ data showed the best coherence with measured water temperatures using: (i) the modified Epstein et al. (1951) relationship as given in O'Brien et al. (2006); or (ii) the Kim & O'Neil (1997) relationship corrected for acid reaction fractionation (Böhm et al., 2000; Affek et al., 2008) (Tables 2 and 3). It is notable that other relationships gave less faithful replication of measured temperatures, including the Hays & Grossman (1991) relationship which was specifically formulated for meteoric calcites, and the Coplen (2007) relationship.

The mean seasonal $\delta^{18}\text{O}_{\text{water}}$ of the River Piedra from 2000 to 2012 (Osácar et al., 2013, 2016) was -8.6‰ VSMOW in cool periods and -8.5‰ VSMOW in warm periods, with 1σ for the whole sample set being 0.44 ($n = 134$; Osácar et al., 2013). These means were used in the temperature

equations as the best representation of likely water isotopic composition. Temperatures derived from both equations are similar (Tables 2 and 3), but for simplicity, this study reports values from just the ‘Epstein relationship’ in the text.

RESULTS

Isotopic and petrographic data for the river deposits are discussed in Osácar et al., (2016) and Arenas & Jones (2017). This paper provides only contextual information to help interpret the pipe data and the new high-resolution isotopic data.

Macroscopic and microscopic features: riverine samples

The riverine tufa stromatolites developed on the tablets are essentially pure calcite, appearing as alternating dense and porous composite laminae (Fig. 2C) formed of cyanobacterial calcite tubes with less common macrocrystalline laminae (Fig. 4A to C). The dense (up to 15 mm thick) and porous composite laminae (up to 12 mm thick) are formed of several dense and porous single laminae, 0.2 to 5.0 mm thick (Fig. 4A; see also Arenas & Jones, 2017). The tubes, formed by calcite precipitation around filamentous cyanobacteria, primarily *Phormidium incrustatum* (Berrendero et al., 2016), are arranged in fan-shaped and sub-parallel bodies, forming palisades (Fig. 4C and D). The porous composite laminae are dominant in the cool period deposits and the dense composite laminae are dominant in the warm period deposits. Each dense and each porous composite lamina represents a few months (typically up to about six months) of deposition (Arenas & Jones, 2017). The flat to slightly undulose macrocrystalline laminae and lenses are up to 1.7 mm thick, formed of elongate crystals (up to 1 mm long and 200 µm wide). These macrocrystalline laminae are conspicuous at the base of most cool period deposits, but are also present in warm period deposits (Fig. 4A to C). Macrocrystalline laminae have sharp bases, particularly in the cool period deposits (Fig. 4B), often over erosional surfaces.

$\delta^{18}\text{O}$ and $\delta^{13}\text{C}$: riverine samples

The $\delta^{18}\text{O}$ values from the two river tablets (P-14 and P-16) range from -9.4 to -7.1‰ VPDB, with means of -8.2 (P-14) and -8.3 (P-16; see Fig. 7A; Appendix S1). There is a clear cyclic variation in $\delta^{18}\text{O}$ of around 1‰ through time. The two records have near identical mean $\delta^{18}\text{O}$ for the warm and cool period deposits (composite means: $\delta^{18}\text{O}_{\text{warm}} = -8.7$ and $\delta^{18}\text{O}_{\text{cool}} = -7.8$ ‰ VPDB). The $\delta^{13}\text{C}$ values of P-14 and P-16 range from -8.5 to -6.9‰ VPDB, with means of -7.8 (P-14) and -7.6 (P-16).

Variation in $\delta^{13}\text{C}$ values is mostly not related to the $\delta^{18}\text{O}$ cyclicity, although it does show a 1‰ drift to less negative values after September 2009 to the end of the record.

Macroscopic and microscopic features: pipe deposit

The deposit, composed wholly of calcite, coated slightly less than the lower half of the pipe, with only slightly decreasing thickness (7.1 to 6.5 cm) downpipe. The deposit is strongly laminated, the laminae inheriting the concave pipewall shape (Fig. 3). The upper (younger) laminae laterally overlap the older ones, and in their downstream part display gently regular asymmetrical undulations (ripple-like forms) that indicate flow direction (Fig. 3A). The cross-sectional area implies that water depth was initially *ca* 15 to 18 cm shallowing to 6 to 7 cm over time (Fig. 3B).

Alternating dark and light laminae are conspicuous in hand specimen (Fig. 3B) which under the optical microscope correspond respectively: to (i) porous and/or light large-crystal (sparitic) laminae (1.3 to 3.8 mm thick; mean = 2.4 mm), hereafter type A laminae; and (ii) dense and/or dark, micritic to microsparitic laminae (1.0 to 3.3 mm thick; mean = 2.1 mm), hereafter type B laminae (Fig. 5A to D). Both lamina types can be single or composite; the latter consisting of two to four laminae that differ from each other in crystal size and colour. Composite laminae are more common in type B.

Type A laminae exhibit columnar sparitic crystals 0.5 to 2.5 mm long, although in some laminae a decrease in crystal size occurs in the uppermost part. The spar crystals are grouped in adjacent fan-shaped and upright parallel bodies, forming palisades (Fig. 5A to D and H). Micrite, either forming

thin laminae or as irregular patches between the elongate crystals, may be present (Fig. 5A and D) as can irregular cavities (microns to millimetres long), either at random or aligned parallel to lamination.

Type B laminae are typically micritic to microsparitic, although larger crystals up to 1.3 mm long may be present, typically occurring in groups of limited continuity among the finer textures (Fig. 5E and F). Type B composite laminae consist of alternating dark (dominant) and light laminae (Fig. 5A and C). Microbial filamentous tubes, parallel to crystal length are more abundant in the type B laminae, although present in both lamina types (Fig. 5C and G). Their presence in the pipe deposit, indicates formation, at least in part, by calcification of cyanobacterial mats. Filaments are grouped in adjacent fan-like and bush-like bodies, which can form extensive palisades, or occur as isolated masses within the coarse-crystal structures (Fig. 5E and F).

Boundaries between lamina types A and B can be sharp or gradational, but always with flat, slightly wavy and multiconvex bounding surfaces (Fig. 5A to C). In many cases, sharp A-B boundaries coincide with a thin layer (20 to 50 μm thick) of much smaller calcite crystals (Fig. 5A and B) or with higher-porosity at the top of the type A lamina (Fig. 5B). In other cases, A-B boundaries show gradual increase in abundance of micrite and microspar upward. Most B-A boundaries are gradational and there is very little evidence of erosion. However, the boundary between lamina 6 and 7 (Fig. 5A) appears corroded by dissolution, the potential for which is supported by negative SI_{calcite} in some cool periods (for example, December 2005; Appendix 1 in Arenas et al., 2014).

$\delta^{18}\text{O}$ and $\delta^{13}\text{C}$: pipe deposit

The $\delta^{18}\text{O}$ in the pipe deposit ranges from -9.0 (Tbx-20) to -7.7 (Tbx-31), with a mean of -8.3‰ VPDB (Table 2; Appendix S2). The $\delta^{18}\text{O}$ values show *ca* 1.5‰ scale cyclicity related to lamina type; least negative values are in type A laminae (mean $\delta^{18}\text{O}_{\text{lam A}} = -8.0\text{‰}$ VPDB) and more negative values in type B laminae (mean $\delta^{18}\text{O}_{\text{lam B}} = -8.7\text{‰}$ VPDB; Fig. 6). $\delta^{13}\text{C}$ variability ranges from -8.7 (Tbx-21) to -7.8 (Tbx-2), with a mean of -8.3‰ VPDB (Table 2; Appendix S2). Mean $\delta^{13}\text{C}$ values are very

similar in both lamina types (mean $\delta^{13}\text{C}_{\text{lam A}} = -8.3\text{‰}$ VPDB and mean $\delta^{13}\text{C}_{\text{lam B}} = -8.2\text{‰}$ VPDB; Fig. 6B), although in parts of the record there is a weak $<0.5\text{‰}$ cyclicity of opposite sign to $\delta^{18}\text{O}$ cyclicity (Fig. 6B and C). Assuming that cyclic variation in $\delta^{18}\text{O}_{\text{calcite}}$ is biannual, and in the absence significant discontinuities, the record in the pipe begins in cool period 1993/1994 (i.e. winter 1993/1994) and spans 15 years to the cool period 2008/2009 (Fig. 7).

High-resolution sampling $\delta^{13}\text{C}$ and $\delta^{18}\text{O}$ data

The high-resolution sampling (HRS) $\delta^{13}\text{C}$ and $\delta^{18}\text{O}$ values are entirely consistent with the bulk data (for example, compare Figs 7 and 8, and Table 3, lamina 30 in the pipe deposit, and cool period 2008/2009 in the river deposit). $\delta^{18}\text{O}$ values show cyclical change in both the pipe and the river data, with most negative values in the warm periods and least negative in the cool periods. A marked break occurs in the river record (not seen in the pipe) during cold period 2008/2009 associated with a sharp decrease of 0.8‰ that follows a maximum in $\delta^{18}\text{O}$ (i.e. erosional hiatus in Fig. 8A). Variations in $\delta^{13}\text{C}$ values are mostly not synchronous with those in $\delta^{18}\text{O}$, but do show partial patterns of both co-cyclicity and opposite sign cyclicity in different sections of the records (Fig. 8).

$\delta^{18}\text{O}$ -derived temperature

To estimate water temperatures (T_w) from $\delta^{18}\text{O}_{\text{calcite}}$, this study makes the reasonable assumption that the mean seasonal $\delta^{18}\text{O}_{\text{water}}$ values, with low statistical variability over time (see above), are representative of the likely actual seasonal $\delta^{18}\text{O}_{\text{water}}$ at any given time. This being so, then changes in $\delta^{18}\text{O}_{\text{calcite}}$ should mostly reflect changes in water temperature (cf. Matsuoka et al., 2001).

In the river, T_w calculated from the 'Epstein relationship' using mean $\delta^{18}\text{O}_{\text{water}}$ ranged from 17.6 to 10.1°C , with a mean of 16.2°C for the warm period deposits, and 11.8°C for the cool period deposits (difference warm versus cool $T_w = 4.4^\circ\text{C}$) (Table 2). Mean T_w calculated using HRS $\delta^{18}\text{O}_{\text{calcite}}$ values

(Fig. 8; Table 3; Appendix S3) ranged from 11.6°C (cool 2008/2009) to 15.5°C (warm 2009) (Table 3), with a difference of 3.6°C.

Water temperature estimates, derived from the mean $\delta^{18}\text{O}_{\text{water}}$ ranged from 17.0 to 12.1°C, with a mean of 16.1°C for type B laminae, and a mean of 12.7°C for type A laminae (Table 2). Mean Tw calculated using HRS $\delta^{18}\text{O}_{\text{calcite}}$ values (Fig. 8; Table 3; Appendix S4) ranged from 11.7°C (type A lamina 31) to 15.0°C (type B lamina 30) (Table 3), with a difference of 3.1°C. The data in Table 3 show that laminae 30 and 31, where HRS was complete, give very similar calculated mean Tw regardless of sample resolution.

The HRS $\delta^{18}\text{O}_{\text{calcite}}$ -derived Tw demonstrate the gradual change in water temperature with time in both the pipe and the river (Fig. 8). The exception is the break in cool period 2008/2009 river $\delta^{18}\text{O}_{\text{calcite}}$, which is followed by a jump in Tw (3.7°C) following a pre-break minimum.

DISCUSSION

$\delta^{18}\text{O}_{\text{calcite}}$ -derived temperature variability

River record (1999 to 2012)

The mean riverine range of Tw estimated from bulk $\delta^{18}\text{O}_{\text{calcite}}$ is 4.4°C, while the measured Tw range between warm (spring + summer) and cool (autumn + winter) periods was 4.6°C (4.05°C between spring + summer and autumn; Table 2). The river tufa stromatolites are thus essentially a complete record of the actual Tw variation, with only the coldest times, when calcite precipitation mass decreased to minimum, likely to be unrepresented. The cool period deposits thus mostly formed in autumn and perhaps milder winter conditions. The gradual increase in calculated Tw with time is parallel to the T_{air} trend, approximately 1.9°C change in both Tw and T_{air} from cool period 1999 to 2000 to warm period 2012 (Fig. 7B and C).

Differences between actual and calculated Tw from HRS $\delta^{18}\text{O}_{\text{calcite}}$ in the P-14 record (Fig. 8; Table 3) are similar or slightly larger in warm periods (up to 0.3°C) than in cool periods (0.3°C versus autumn + winter and 0.2°C versus autumn). The maximum and minimum calculated Tw (17.3°C and 10.4°C) also coincide with the maximum and minimum monthly measured Tw (17.2°C and 10.4°C). The erosional hiatus affecting the continuity of the HRS P-14 cool 2008/2009 data (Fig. 8A) occurred under very high discharge conditions (fig. 3 in Arenas et al., 2014). The break is followed by a sudden 3.7°C temperature increase, which may have biased the above Tw comparison.

Pipe record (1994 to 2009)

The laminae in the pipe show strong evidence of calcification associated with filamentous cyanobacterial mats (Fig. 5), type B laminae corresponding to higher calculated temperatures and thus forming mostly in spring and summer, hereafter type B (warm) laminae. Type A laminae correspond broadly to the cool season deposits [hereafter type A (cool) laminae], perhaps mostly forming in the autumn and part of winter, but also extending into late spring in some years (for example, until June, as reflected by calculated Tw in lamina 29; Fig. 8D).

The calculated bulk Tw difference between types A and B laminae (Tw = 3.4°C) is *ca* 1°C smaller than the mean measured Tw 4.7°C difference between spring + summer and autumn + winter (4.6°C between spring + summer and autumn) (Table 2). Moreover, the mismatch between Tw from HRS $\delta^{18}\text{O}_{\text{calcite}}$ and actual Tw is larger in the cool period (calculated Tw is up to 0.4°C higher) than in the warm period (calculated Tw is 0.3°C lower) (Table 3). These mismatches are not likely to have been caused by incomplete summer records: (i) because summer water flow is continuous with high SIC (Table 1); and (ii) because gradual changes in both petrographic fabric and HRS isotope compositions from type B to type A laminae (Figs 5B and 8) reflect continuous deposition. It is suspected that an incomplete winter temperature signature is likely to explain the difference as discussed below.

Synchronous records (1999 to 2009)

The HRS synchronous isotopic records (cool 2008/2009 and warm 2009 river periods versus laminae 30 and 31 in the pipe) show close parallelism between measured and calculated T_w change with time, including coincidence between several minimum and maximum values (Fig. 8; Table 3). Moreover, the ‘bulk’ synchronous data (cool period 1999 to 2000 to cool period 2008/2009) in the pipe and in the river (Table 2; Fig. 7) yield reasonable correspondence with calculated warm period T_w (highest difference is 0.6°C). There is, however, *ca* 1°C mismatch (0.6 to 1.8°C) in the cool period data, a disparity that is more marked (up to 1.8°C) in the pipe data comparisons (Table 2). The calculated T_w range between cool and warm periods is smaller in the pipe (calculated T_w range = 3.3°C) than in the river (calculated T_w range = 4.5°C), and both are smaller than the actual T_w range of 4.7°C, from hourly measurements (available 2007 to 2009 data).

The combined information shows that $\delta^{18}\text{O}_{\text{calcite}}$ records in the river and in the pipe reflect almost the full seasonal T_w range. The cool period data mismatch, especially in the pipe, suggests severe reduction or cessation of deposition in the coldest winter periods when T_w is <10°C (see also Matsuoka et al., 2001; Brasier et al., 2010; Osácar et al., 2013). Effects may be most noticeable in the pipe because the depositional masses are smaller and thus below bulk sample resolution. The decreasing trend in the ‘bulk’ calculated T_w in the pipe (approximately 0.5°C) highlights this issue (Fig. 7D); it clearly opposes the ‘bulk’ calculated T_w from the river, which increases *ca* 1.2°C over the same time span (Fig. 7B), as does the measured T_{air} data trend (Fig. 7C).

These results show that accurate seasonal temperature records can be recovered from tufas forming at deposition rates between 5.6 to 10.8 mm over six months using either the Epstein et al. (1951) or Kim & O’Neil (1997) temperature formulations (see also Brasier et al., 2010; Osácar et al., 2013; Sun et al., 2014). The findings of this study support those of Sun et al. (2014) on Chinese travertines, and Zavadlav et al. (2016) in the Slovenian River Krka tufas. Both these deposits have high calcite precipitation rates, comparable to the Piedra River, and in both cases the tufa–water isotope fractionation factors were close to the laboratory-derived curve of Kim & O’Neil (1997), the smallest

Tw differences in the Krka deposits (1.2 to 3.8°C higher) being obtained using the Epstein et al. (1951) equation.

High calcite precipitation rates have been linked by some workers to isotopic disequilibrium effects on $\delta^{18}\text{O}_{\text{calcite}}$ (e.g. Wang et al., 2014; Sun et al., 2014; Watkins et al., 2014; Zavadlav et al., 2016). While kinetic effects of this type cannot be ruled out, the good fit between measured Tw and $\delta^{18}\text{O}_{\text{calcite}}$ -calculated Tw from both bulk and HRS sampling in this work indicate that temperature is the principal control on isotopic data. The Epstein et al. (1951) or Kim & O'Neil (1997) formulations are an accurate description of the temperature dependence of the fractionation factor at the observed growth rates, as indicated in some experimental studies (Watkins et al., 2014).

Lamination, texture and seasonality

Mean seasonal tufa deposition rates in the pipe were 2.1 mm (type B 'warm' laminae) and 2.4 mm (type A 'cool' laminae), much lower than the corresponding river rates (10.8 mm, warm periods; 5.6 mm, cool periods). In part, this is caused by different flow conditions: in the pipe, water depth was greater, with a smooth floor, minimizing turbulence and any corresponding CO₂ degassing that forces calcite precipitation.

The pipe deposit probably also suffered more discontinuous growth, especially in winter, caused by low temperatures and low illumination, inhibiting cyanobacterial growth as autumn progressed to winter. Under limited cyanobacterial growth, calcite precipitation can occur outside the biofilm (extra-EPS sites of Pedley, 2014), favouring abiogenic precipitation of large calcite spar crystals (Pedley, 2014). Such calcification may prevail during autumn and winter, favouring calcite spar growth on and into the cyanobacterial mat (cf. Pentecost, 1987, 1988); such growth might even penetrate underlying type B laminae resulting in a gradational boundary between lamina types. This process can also occur at other times of the year, explaining the observation of large crystals in some type B laminae. In-lamina precipitation of this type will contribute to: (i) underestimation type B

‘warm’ lamina deposition rate; and (ii) higher than expected type A ‘cool’ lamina $\delta^{18}\text{O}_{\text{calcite}}$ -derived Tw (Figs 7 and 8).

This ‘blurring’ of seasonal growth is much less evident in the riverine tufa stromatolites, where sharp bases below macrocrystalline laminae suggest breaks in the cyanobacterial growth at discrete times (Arenas & Jones, 2017) caused by either erosion or seasonally low temperatures (Arp et al., 2010).

Lamina boundaries and $\delta^{18}\text{O}_{\text{calcite}}$ reversals

In both the pipe and river HRS $\delta^{18}\text{O}_{\text{calcite}}$ data, seasonal maxima and minima (Fig. 8), that define ‘reversal’ in temperature, occur within laminae, not at lamina boundaries. This pattern probably reflects changes in calcite precipitation rates, as proposed for a French Eemian tufa stromatolite (Dabkowski et al., 2015), due to intra-seasonal changes in temperature, pCO_2 and Ca content that affect $\text{SI}_{\text{calcite}}$ and calcite precipitation rate. The fact that points of ‘reversal’ do not coincide with lamina boundaries suggests that marked seasonal hiatuses caused by either summer drought or extreme winter cold (cf. Brasier et al., 2010) were not present. Rather, gradual re-establishment of cyanobacterial growth in spring, led to largely progressive change in the pipe from type A to type B laminae consistent with a seasonal Mediterranean climate.

Stable carbon isotopes

Variations in $\delta^{13}\text{C}$ values are mostly not synchronous with those in $\delta^{18}\text{O}$, regardless of sample resolution or site of deposition. Apparent partial patterns of co-cyclicity and opposite sign cyclicity are not consistent and may simply be random. Absence of seasonal $\delta^{13}\text{C}_{\text{calcite}}$ patterns in tufas is common, caused by the number of conflicting parameters that affect the signal (Andrews et al., 1997; Lojen et al., 2004; Andrews, 2006; Osácar et al., 2013). The main points worthy of comment are:

- 1 Lower river $\delta^{13}\text{C}_{\text{calcite}}$ values occur mainly in the cool periods, perhaps due to diminished CO_2 degassing under cool conditions with decreased photosynthetic CO_2 uptake (Pentecost, 2005; Andrews, 2006).
- 2 The marked increase in $\delta^{13}\text{C}_{\text{calcite}}$ from warm 2009 to warm 2012 (Fig. 7A) coincides with an increase of water $\delta^{13}\text{C}_{\text{DIC}}$ values (Osácar et al., 2016). This is caused by an increasingly ^{13}C -rich HCO_3^- supply from the aquifer over time (cf. Leng & Marshall, 2004; Andrews, 2006; Osácar et al., 2016), driven by decreased aquifer recharge from 2009 onwards (see figs 2 and 3 in Arenas et al., 2014).
- 3 The 'bulk' pipe $\delta^{13}\text{C}_{\text{calcite}}$ values (mean $\delta^{13}\text{C} = -8.4\text{‰}$) are slightly more negative than the corresponding, synchronous (1999 to 2009), river data (mean $\delta^{13}\text{C} = -7.9\text{‰}$; Table 2; Fig. 7). Moreover, the difference (0.5‰) is smaller in warm periods (0.3‰) than cool periods (0.6‰). This may reflect: (i) less CO_2 degassing due to relatively low turbulence in the pipe cool periods (cf. Sürmelihindi et al., 2013); and (ii) the effect of low illumination on photosynthetic CO_2 -uptake in the pipe, even though evidence for microbial influence on $\delta^{13}\text{C}_{\text{calcite}}$ in most riverine tufas (Pentecost & Spiro, 1990) is usually negligible.

CONCLUSIONS

Detailed calibration of stable isotope records in riverine tufa stromatolites requires a well-characterized system with high-resolution water temperature data and predictable water isotopic composition. The River Piedra (north-east Spain) is an ideal site; a twelve-year record in river-bed tufa stromatolites was recovered in this study, along with a partly overlapping fifteen-year record of tufa accumulations in a drainage pipe. Data from this study confirm that both deposits record essentially the full actual seasonal water temperature (T_w) range.

- Most importantly, this study found that the Epstein et al. (1951) and Kim & O'Neil (1997) formulas for T_w calculation from equilibrium calcite $\delta^{18}\text{O}$ compositions were most appropriate for the River Piedra where tufa deposition rates are high, with means between 5.6

mm and 10.8 mm in six months. These findings support those of Sun et al. (2014) on Chinese travertines, and Zavadlav et al. (2016) in the Slovenian River Krka tufas. While this study cannot rule out the minor kinetic effects noticed in systems with high rates of calcite precipitation (e.g. Sun et al., 2014; Wang et al., 2014; Watkins et al., 2014; Zavadlav et al., 2016), the good fit between measured T_w and $\delta^{18}O_{\text{calcite}}$ -calculated T_w from both bulk and high-resolution sampling in this work indicate that temperature is the principal control on isotopic data.

- Only the coldest winter temperatures (in this case $T_w < 10^\circ\text{C}$), when calcite precipitation mass decreases to minimum, are probably unrepresented in tufa stromatolite records.
- Textural and deposition rate variability between the river and pipe settings are caused by differences in flow velocity and illumination. In the river, calcification of growing cyanobacterial mat occurred throughout the year, whereas in the pipe, cessation of cyanobacterial growth in winter allowed more abiogenic calcification.
- Reversals in T_w occur within laminae, not at lamina boundaries, a pattern consistent with progressive increase in calcite precipitation rate as cyanobacterial growth re-established in spring.

ACKNOWLEDGEMENTS

This study was funded by projects CGL2009-09216/CLI and CGL2013-42867 of the Spanish Government and European Regional Funds. This work fits the objectives of the ‘Continental Sedimentary Basins Analysis’ and Geotransfer research groups (Aragón Government and University of Zaragoza, and European Regional Funds). Dr. Sancho Marcén is kindly acknowledged for his scientific help. We thank the personnel of the *Servicio de Preparación de Rocas y Materiales Duros* and Scanning Electron Microscopy (*Servicio General de Apoyo a la Investigación-SAI*) of the University of Zaragoza, as well as technicians in the Scanning

Electron Microscopy Laboratory of the Department of Earth and Atmospheric Sciences at the University of Alberta for their help. We are grateful to the management and staff of the Monasterio de Piedra Natural Park for facilitating our fieldwork. Two anonymous reviewers and Associate Editor Dr. A. Brasier provided interesting comments and questions that helped improve the manuscript.

REFERENCES

- Affek, H.P., Bar-Matthews, M., Ayalon, A., Matthews, A. and Eiler, J.M.** (2008) Glacial/interglacial temperature variations in Soreq cave speleothems as recorded by ‘clumped isotope’ thermometry. *Geochim. Cosmochim. Acta*, **72**, 5351–5360
- Andrews, J.E.** (2006) Palaeoclimatic records from stable isotopes in riverine tufas: Synthesis and review. *Earth-Sci. Rev.*, **75**, 85-104.
- Andrews J.E., Riding R. and Dennis P.F.** (1997) The stable isotope record of environmental and climatic signals in modern terrestrial microbial carbonates from Europe. *Palaeogeogr. Palaeoclimatol. Palaeoecol.*, **129**, 171-189.
- Andrews, J.E. and Brasier, A.T.** (2005) Seasonal records of climatic change in annually laminated tufas; short review and future prospects. *J. Quaternary Sci.*, **20**, 411-421.
- Arenas, C., Vázquez-Urbez, M., Auqué, L., Sancho, C., Osácar, M.C. and Pardo, G.** (2014) Intrinsic and extrinsic controls of spatial and temporal variations in modern fluvial tufa sedimentation: A thirteen-year record from a semi-arid environment. *Sedimentology*, **61**, 90–132. doi: 10.1111/sed.12045
- Arenas, C. and Jones, B.** (2017) Temporal and environmental significance of microbial lamination: Insights from Recent fluvial stromatolites in the River Piedra, Spain. *Sedimentology*, **65**. In Press DOI: 10.1111/sed.12365

- Arp, G., Wedemeyer, N. and Reitner, J.** (2001) Fluvial tufa formation in a hard-water creek (Deinschwanger Bach, Franconian Alb, Germany). *Facies*, **44**, 1-22.
- Berrendero, E., Arenas, C., Mateo, P. and Jones, B.** (2016) Cyanobacterial diversity and related sedimentary facies as a function of water flow conditions: Example from the Monasterio de Piedra Natural Park (Spain). *Sed. Geol.*, **337**, 12-28. doi: 10.1016/j.sedgeo.2016.03.003.
- Böhm, F., Joachimski, M.M., Dullo, W.-C., Eisenhauer, A., Lehnert, H., Reitner, J. and Wörheide, G.** (2000) Oxygen isotope fractionation in marine aragonite of coralline sponges. *Geochim. Cosmochim. Acta*, **64**, 1695–1703. DOI: 10.1016/S0016-7037(99)00408-1
- Brasier, A.T., Andrews, J.E., Marca-Bell, A.D. and Dennis, P.F.** (2010) Depositional continuity of seasonally laminated tufas: Implications for $\delta^{18}\text{O}$ based palaeotemperatures. *Global Planet. Change*, **71**, 160-167.
- Coplen, T.** (2007) Calibration of the calcite-water-oxygen isotope geothermometer at Devils Hole, Nevada, a natural laboratory. *Geochim. Cosmochim. Acta*, **71**, 3948-3957. doi: 10.1016/j.gca.2007.05.028
- Craig, H.** (1965) The measurement of oxygen isotope palaeotemperatures. In: *Stable Isotopes in Oceanographic Studies and Palaeotemperatures* (Ed. E. Tongiorgi), pp. 161– 182. Consiglio Nazionale Della Ricerca. Laboratorio de Geologia Nucleare, Pisa.
- Dabkowski, J., Royle, S.H., Antoine, P., Marca-Bell, A. and Andrews, J.E.** (2015) High-resolution $\delta^{18}\text{O}$ seasonality record in a French Eemian tufa stromatolite (Caours, Somme Basin). *Palaeogeogr. Palaeoclimat. Palaeoecol.*, **438**, 277-284. doi: 10.1016/j.palaeo.2015.08.017
- Day, C.C. and Henderson, G.M.** (2011) Oxygen isotopes in calcite growth under cave-analogue conditions. *Geochim. Cosmochim. Acta*, **75**, 3956–3972.

- Dietzel, M., Tang, J., Leis, A. and Köhler, S.J.** (2009) Oxygen isotopic fractionation during inorganic calcite precipitation — Effects of temperature, precipitation rate and pH. *Chem. Geol.*, **268**, 107–115. doi: 10.1016/j.chemgeo.2009.07.015
- Epstein, S. and Mayeda, T.** (1953) Variation of O¹⁸ content of waters from natural sources. *Geochim. Cosmochim. Acta*, **4**, 213-224.
- Epstein, S., Buchsbaum, R., Lowenstam, H. and Urey, H.C.** (1951) Carbonate-water isotopic temperature scale. *Geol. Soc. Am. Bull.*, **62**, 417–426.
- Fairchild, I.J., Smith, C.L., Baker, A., Fuller, L., Spötl, C., Matthey, D. and McDermott, F.** (2006) Modification and preservation of environmental signals in speleothems. *Earth-Sci. Rev.*, **75**, 105–153. doi: 10.1016/j.earscirev.2005.08.003
- Hays, P.D. and Grossman, E.L.** (1991) Oxygen isotopes in meteoric calcite cements as indicators of continental paleoclimate. *Geology*, **19**, 441-444.
- Kano, A., Hagiwara, R., Kawai, T., Hori, M. and Matsuoka, J.** (2007) Climatic conditions and hydrological change recorded in a high-resolution stable-isotope profile of a recent laminated tufa on a subtropical island, southern Japan. *J. Sed. Res.*, **77**, 59-67. doi:10.2110/jsr.2007.006
- Kele, S, Breitenbach, S.F.M., Capezzuoli, E., Meckler, A.N., Ziegler, M., Millan, I.M., Kluge, T., Deák, J., Hanselmann, K., John, C.M., Yan, H., Liu, Z. and Bernasconi, S.M.** (2015) Temperature dependence of oxygen- and clumped isotope fractionation in carbonates: A study of travertines and tufas in the 6–95 °C temperature range. *Geochim. Cosmochim. Acta*, **168**, 172–192. doi:/10.1016/j.gca.2015.06.032.
- Kim, S.-T. and O'Neil, J.R.** (1997) Equilibrium and non-equilibrium oxygen isotope effects in synthetic carbonates. *Geochim. Cosmochim. Acta*, **61**, 3461-3475.
- Leng, M.J. and Marshall, J.D.** (2004) Palaeoclimate interpretation of stable isotope data from lake sediment archives. *Quaternary Sci. Rev.*, **23**, 811–831. doi: 10.1016/j.quascirev.2003.06.012.

- Lojen, S., Dolenc, T., Vokal, B., Cukrov, N., Mihelci, G. and Papesch, W.** (2004) C and O stable isotope variability in recent freshwater carbonates (River Krka, Croatia). *Sedimentology*, **51**, 361-375. doi: 10.1111/j.1365-3091.2004.00630.x
- Lojen, S., Trkov, A., Scancar, J., Vazquez-Navarro, J.A. and Cukrov, N.** (2009) Continuous 60 year stable isotopic and earth-alkali element records in a modern laminated tufa (Jaruga, River Krka, Croatia); implications for climate reconstruction. *Chem. Geol.*, **258**, 242-250. doi: 10.1016/j.chemgeo.2008.10.013.
- Matsuoka, J., Kano, A., Oba, T., Watanabe, T., Sakai, S. and Seto, K.** (2001) Seasonal variation of stable isotopic compositions recorded in a laminated tufa, SW Japan. *Earth Planet. Sci. Lett.*, **192**, 31-44. doi: 10.1016/S0012-821X(01)00435-6.
- McCrea, J.M.** (1950) On the isotope chemistry of carbonates and a paleotemperature scale. *J. Chem. Phys.*, **18**, 849-587.
- O'Brien, G.R., Kaufman, D.S., Sharp, W.D., Atudorei, V., Parnell, R.A. and Crossey, L.J.** (2006) Oxygen isotope composition of annually banded modern and mid-Holocene travertine and evidence of paleomonsoon floods, Grand Canyon, Arizona, USA. *Quatern. Res.*, **65**, 366-379. doi: 10.1016/j.yqres.2005.12.001.
- Osácar, C., Arenas, C., Vázquez-Urbez, M., Sancho, C., Auqué, L.F. and Pardo, G.** (2013) Environmental factors controlling the $\delta^{13}\text{C}$ and $\delta^{18}\text{O}$ variations of recent fluvial tufas: a 12-year record from the Monasterio de Piedra Natural Park (NE Iberian Peninsula). *J. Sed. Res.*, **83**, 309-322. doi: 10.2110/jsr.2013.27.
- Osácar, M.C., Arenas, C., Auqué, L., Sancho, C., Pardo, G. and Vázquez-Urbez, M.** (2016) Discerning the interactions between environmental parameters reflected in $\delta^{13}\text{C}$ and $\delta^{18}\text{O}$ of recent fluvial tufas: Lessons from a Mediterranean climate region. *Sed. Geol.*, **345**, 126-144. <http://dx.doi.org/10.1016/j.sedgeo.2016.09.004>

- Pedley, M.** (2014) The morphology and function of thrombolitic calcite precipitating biofilms: A universal model derived from freshwater mesocosm experiments. *Sedimentology*, **61**, 22–40. doi: 10.1111/sed.12042.
- Pentecost, A.** (1987) Growth and calcification of the freshwater cyanobacterium *Rivularia haematites*. *Proc. R. Soc. London, B*, **232**, 125–136. DOI: 10.1098/rspb.1987.0064.
- Pentecost, A.** (1988) Growth and calcification of the cyanobacterium *Homeothrix crustacea*. *Microbiology*, **134**, 2665–2671.
- Pentecost, A.** (2005) *Travertine*. Springer-Verlag, Berlin, 445 pp.
- Pentecost, A.** and **Spiro, B.** (1990) Stable carbon and oxygen isotopic composition of calcites associated with modern freshwater cyanobacteria and algae. *Geomicrobiol J.*, **8**, 17–26.
- Sancho, C., Arenas, C., Vázquez-Urbez, M., Pardo, G., Lozano, M.V., Peña, J.L., Hellstrom, J., Ortiz, J.E., Osácar, M.C., Auqué, L. and Torres, T.** (2015) Climatic implications of the Quaternary fluvial tufa record in the NE Iberian Peninsula over the last 500 ka. *Quatern. Res.*, **84**, 398–414. doi: /10.1016/j.yqres.2015.08.003.
- Sun, H., Liu, Z. and Yan, H.** (2014) Oxygen isotope fractionation in travertine-depositing pools at Baishuitai, Yunnan, SW China: Effects of deposition rates. *Geochim. Cosmochim. Acta*, **133**, 340–350. doi: 10.1016/j.gca.2014.03.006
- Tremaine, D.M., Froelich, P.N. and Wang, Y.** (2011) Speleothem calcite formed *in situ*: Modern calibration of $\delta^{18}\text{O}$ and $\delta^{13}\text{C}$ paleoclimate proxies in a continuously-monitored natural cave system. *Geochim. Cosmochim. Acta*, **75**, 4929–4950 doi:10.1016/j.gca.2011.06.00.
- Vázquez-Urbez, M., Arenas, C., Sancho, C., Osácar, C., Auqué, L. and Pardo, G.** (2010) Factors controlling present-day tufa dynamics in the Monasterio de Piedra Natural Park (Iberian Range, Spain): depositional environmental settings, sedimentation rates and hydrochemistry. *Int. J. Earth Sci.*, **99**, 1027-1049. doi:10.1007/s00531-009-0444-2.

Wang, H., Yan, Y. and Liu, Z. (2014) Contrasts in variations of the carbon and oxygen isotopic composition of travertines formed in pools and a ramp stream at Huanglong Ravine, China: Implications for paleoclimatic interpretations. *Geochim. Cosmochim. Acta*, **125**, 34–48. doi: 10.1016/j.gca.2013.10.001

Watkins, J.M., Hunt, J.D., Ryerson, F.J. and DePaolo, D.J. (2014) The influence of temperature, pH, and growth rate on the $\delta^{18}\text{O}$ composition of inorganically precipitated calcite. *Earth Planet. Sc. Lett.*, **404**, 332–343. doi: /10.1016/j.epsl.2014.07.036.

Yan, H., Sun, H. and Liu, Z. (2012) Equilibrium vs. kinetic fractionation of oxygen isotopes in two low-temperature travertine-depositing systems with differing hydrodynamic conditions at Baishuitai, Yunnan, SW China. *Geochim. Cosmochim. Acta*, **95**, 63–78. doi:10.1016/j.gca.2012.07.024

Zavadlav, S., Rozic, B., Dolenc, M. and Lojen, S. (2017) Stable isotopic and elemental characteristics of recent tufa from a karstic Krka River (south-east Slovenia): useful environmental proxies? *Sedimentology*, **64**, 808–831. doi: 10.1111/sed.12328

FIGURE CAPTIONS

Fig. 1. (A) Location of study area in the Iberian Range, north-east Iberian Peninsula. (B) Geological map. (C) Aerial view of the River Piedra across the Monasterio de Piedra Natural Park, with studied field sites.

Fig. 2. (A) Field view, (B) plan view and (C) cross-section of tablet P-14 installed in a small waterfall in the River Piedra (location in Fig. 1C). The stromatolite on tablet P-14 records deposition from October 2006 to September 2009.

Fig. 3. Drainage pipe deposit. (A) Retrieved deposit. (B) Lamination in cross-section Tbx. Note dark and light alternating laminae.

Fig. 4. Photomicrographs of stromatolite on tablets P-14 (A), (B) and (D) and P-18 (C). Optical microscope images (A) and (B) and scanning electron microscopy (SEM) images (C) and (D); using a Carl Zeiss MERLIN™ (Carl Zeiss Group, Jena, Germany) at the *Servicios de Apoyo a la Investigación* of the University of Zaragoza (Spain), and a JEOL 6301FXV (JEOL, Tokyo, Japan) at the Department of Earth and Atmospheric Sciences of the University of Alberta (Canada); both were operated at 3 to 5 kV and 150 to 500 pA. (A) Alternating porous and dense composite laminae and macrocrystalline lamina at the base. (B) Macrocrystalline laminae, the initial deposit on the blank tablet (at the base) and on the subsequent dense lamina (first deposit of the 2004/2005 cool period). (C) Sharp contact between dense lamina (cyanobacterial tubes) and macrocrystalline lamina (abiogenic columnar crystals) within the 2008/2009 cool deposit. (D) Detail of a dense lamina made of cyanobacterial tubes (warm 2004 period).

Fig. 5. Photomicrographs of the pipe deposit: (A) to (F) optical microscope; (G) to (H) scanning electron microscope (SEM). (A) and (B) Alternating light (larger crystals) and dark (smaller crystals) laminae, i.e. types A and B, respectively. Sharp and gradual boundaries between laminae are marked by continuous and dashed lines, respectively. Note the dissolution features in lamina 6, and the composite character of laminae 8 and 10. Note in lamina 9 the presence of large elongate crystals (arrowed) that grew (or overgrew) within the sediment (aggradational neomorphism). (C) Composite

type B lamina consisting of single microspar and micrite laminae. Note the presence of cyanobacterial filaments (arrows). (D) Cyanobacterial filaments forming adjacent bush-like bodies in laminae of types A and B (n. 21 and 22). (E) Bush-like cyanobacterial-filament bodies in a type B lamina (n. 18), followed by a type A lamina (n. 19). Note in lamina 18 the presence of large elongate crystals (arrowed) that grew (or overgrew) within the sediment. (F) Detail of a bush-like cyanobacterial body in (E). (G) Calcite tubes formed by calcite precipitation around cyanobacterial filaments (decayed), in a type B lamina (n. 8). (H) Columnar calcite crystals in a type A lamina (n. 3).

Fig. 6. Bulk sampling stable isotopes of the pipe deposit. (A) and (D) Cross-section images with indication of sampled points and lamina numbers. (B) and (C) $\delta^{13}\text{C}$ and $\delta^{18}\text{O}$ values (‰ VPDB) plotted through time. Each number on the photographs matches the same number on the column between plots (B) and (C). Grey and white bands in plots (B) and (C) do not line up exactly with laminae in (A) and (D) – see Supporting Information.

Fig. 7. Bulk sampling stable isotopes, calculated Tw (using ‘Epstein relationship’, with $\delta^{18}\text{O}_{\text{water}} = -8.5$ ‰ VSMOW for cool and warm periods) and measured Tw (from hourly values available from June 2007 to September 2012) of the river (A) and (B) and pipe (D) and (E) deposits. (C) Monthly air temperature values averaged from data provided by *Agencia estatal de Meteorología* at the La Tranquera and Milmarcos meteorological stations, *ca* 700 m and 1050 m above sea level, respectively.

Fig. 8. HRS stable isotopes of selected, partially synchronous intervals in the river (A) and pipe deposit (E; laminae 28 to 31). See Figs 2C and 6A for location of intervals. (B) and (D) Calculated Tw for each case (using ‘Epstein relationship’, with $\delta^{18}\text{O}_{\text{water}} = -8.5$ ‰ VSMOW for cool and warm periods). (C) Hourly and monthly Tw from hourly measures available from June 2007 to September 2012. (F) Photomicrograph (optical microscope) of laminae 28 to 31 in the pipe deposit.

TABLES

Table 1. Main hydrophysical and hydrochemical parameters, and deposition rates measured in two stromatolite-forming sites (P-14 and P-16) in the Monasterio de Piedra Natural Park (compiled from Arenas et al., 2014).

Table 2. Mean values of $\delta^{13}\text{C}_{\text{calcite}}$ and $\delta^{18}\text{O}_{\text{calcite}}$ and calculated Tw, using equations 1 ('Epstein relationship'; from Epstein et al., 1951) and 2 (Kim & O'Neil, 1997), of two stromatolite deposits in the river (averaged P-14 and P-16 from Osácar et al., 2016) and drainage pipe deposits. (In both equations, $\delta^{18}\text{O}_{\text{water}} = -8.6$ for cool periods and $\delta^{18}\text{O}_{\text{water}} = -8.5$ in warm periods). Measured Tw from hourly data from June 2007 to September 2012.

Table 3. Water temperature (Tw) calculated using $\delta^{18}\text{O}_{\text{calcite}}$ obtained from bulk and HRS in the pipe (laminae 28 to 31) and in the river deposits (warm 2007 to warm 2009), using equations 1 ('Epstein relationship'; from Epstein et al., 1951) and 2 (Kim & O'Neil, 1997). (In both equations, $\delta^{18}\text{O}_{\text{water}} = -8.6$ for cool periods and $\delta^{18}\text{O}_{\text{water}} = -8.5$ in warm periods). Measured Tw from hourly data from June 2007 to September 2012.

SUPPORTING INFORMATION

Table S1. Averaged $\delta^{13}\text{C}_{\text{calcite}}$ and $\delta^{18}\text{O}_{\text{calcite}}$ data from bulk sampling in river deposits at sites P-14 and P-16 (compiled from Osácar et al., 2016).

Table S2. $\delta^{13}\text{C}_{\text{calcite}}$ and $\delta^{18}\text{O}_{\text{calcite}}$ data from bulk sampling in the drainage pipe deposit.

Table S3. HRS $\delta^{13}\text{C}_{\text{calcite}}$ and $\delta^{18}\text{O}_{\text{calcite}}$ data in deposit at site P-14, representing warm 2008 (samples 51 to 64), cool 2008/2009 (samples 39 to 50) and warm 2009 (samples 1 to 38) deposition. See Fig. 2C.

Table S4. HRS $\delta^{13}\text{C}_{\text{calcite}}$ and $\delta^{18}\text{O}_{\text{calcite}}$ data in the pipe deposit (laminae 28 to 31). Lamina 28: samples 58 to 75. Lamina 29: samples 41 to 57. Lamina 30: samples 23 to 40. Lamina 31: samples 1 to 22.

		P-14	P-16	Mean P-14 and P-16
Temperature (°C) (from sampling time measurements) (1)	June	17.1	17.2	17.1
	January	10.0	9.9	9.6
	All	13.3	13.3	13.3
Temperature (°C) (from hourly measurements) (2)	Warm	-	-	15.71
	Cool	-	-	11.07
	Yearly	-	-	13.39
pH (sampling time) (1)	June	8.16	8.16	8.18
	January	7.94	7.97	7.93
	All	8.05	8.09	8.07
Alk. (mg/L HCO ³⁻) (1)	June	264.11	262.54	263.33
	January	268.42	266.40	267.41
	All	266.15	264.37	265.26
Ca (mg/L) (1)	June	84.42	82.46	83.44
	January	85.41	84.31	84.92
	All	84.94	83.34	84.14
TIC (mg/L) (1)	June	52.20	51.24	51.48
	January	54.60	53.76	54.24
	All	53.16	52.44	52.80
Log PCO ₂ (1)	June	-2.82	-2.87	-2.85
	January	-2.63	-2.67	-2.65
	All	-2.72	-2.77	-2.75
SI calcite (1)	June	+0.86	+0.89	+0.88
	January	+0.56	+0.60	+0.56
	All	+0.70	+0.74	+0.72
PWP (mmol/cm ² /s) (1)	June	2.67·10 ⁻⁷	2.78·10 ⁻⁷	2.73·10 ⁻⁷
	January	1.16·10 ⁻⁷	1.05·10 ⁻⁷	1.02·10 ⁻⁷
	All	1.87·10 ⁻⁷	1.96·10 ⁻⁷	1.92·10 ⁻⁷
Flow velocity (cm/s) (3)	Warm	221.5	132.0	176.75
	Cool	227.7	135.4	181.55
Water depth (cm) (3)	Warm	6.5	5.8	6.15
	Cool	7.4	8.8	8.1
Deposition rate (mm) (3)	Warm	9.82	11.15	10.48
	Cool	6.20	5.38	5.79
	Yearly	16.02	16.53	16.27

(1) June 2003 to September 2012. (2) June 2007 to September 2012.

(3) November 1999 to September 2012.

Cool: Autumn and Winter seasons. Warm: Spring and Summer seasons

Table 1

Table 2

	Mean $\delta^{13}\text{C}_c$ (‰ V-PDB)	Mean $\delta^{18}\text{O}_c$ (‰ V-PDB)	Calculated water temperature (°C)		Measured water temperature (°C)	
			EPSTEIN	KIM-O'NEIL	Tw1	Tw2
RIVER (MERGED P14+P16): 1999-2012						
Cool periods	-7.71	-7.78	11.82	11.06	11.07	11.66
Warm periods	-7.84	-8.71	16.25	15.79	15.71	15.71
Difference	-0.13	-0.93	4.43	4.73	4.64	4.05
RIVER (MERGED P14+P16): 1999-2009						
Cool periods	-7.82	-7.73	11.61	10.84	10.85	10.98
Warm periods	-7.95	-8.69	16.16	15.68	15.57	15.57
Difference	-0.13	-0.95	4.55	4.84	4.72	4.59
DRAINAGE PIPE: 1994-2009						
Type A laminae	-8.35	-7.98	12.66	11.98	10.85	10.98
Type B laminae	-8.19	-8.68	16.11	15.65	15.57	15.57
Difference	0.16	-0.70	3.45	3.67	4.72	4.59
DRAINAGE PIPE: 1999-2009						
Type A laminae	-8.43	-7.97	12.66	11.90	10.85	10.98
Type B laminae	-8.29	-8.65	16.01	15.53	15.57	15.57
Difference	0.13	-0.69	3.35	3.63	4.72	4.59

Cool = Autumn + Winter Warm = Spring + Summer

Tw1: Spring + Summer and Autumn + Winter

Tw2: Spring + Summer and Autumn

Cool $\delta^{18}\text{O}_{\text{water}}$ = -8.6 ‰ V-SMOW

Warm $\delta^{18}\text{O}_{\text{water}}$ = -8.5 ‰ V-SMOW

Table 3

	Measured water temperature (°C)		Pipe Lamina number	Calculated water temperature (°C)				Calculated water temperature (°C)			
				Drainage pipe deposit				Stromatolite river deposit (tablet P-14)			
	Tw1	Tw2		Bulk sampling		High resol. sampling		Bulk sampling		High resol. sampling	
			EPSTEIN	KIM-O'NEIL	EPSTEIN	KIM-O'NEIL	EPSTEIN	KIM-O'NEIL	EPSTEIN	KIM-O'NEIL	
Warm 2009	15.84	15.84									
Cool 2008-09	11.29	11.45	31	11.69	10.93	11.73	10.97	10.91	10.07	11.61	10.84
Warm 2008	15.27	15.27	30	15.19	14.68	15.01	14.49	15.19	14.68	14.93	14.40
Cool 2007-08	10.48	10.51	29	12.02	11.29	11.86*	11.11*	10.75	9.89		
Warm 2007	16.49	16.49	28	15.54	15.05	14.80*	14.26*	15.72	15.23		
Mean warm periods	15.88	15.88		15.36	14.86	14.90	14.37	15.59	15.09	15.23	14.72
Mean cool periods	10.89	10.98		11.86	11.11	11.80	11.04	10.83	9.98	11.61	10.84
Difference warm-cool	5.00	4.90		3.51	3.75	3.11	3.34	4.76	5.11	3.62	3.89

Warm = Spring + Summer

Cool = Autumn + Winter

* Incomplete record (see Fig. 8)

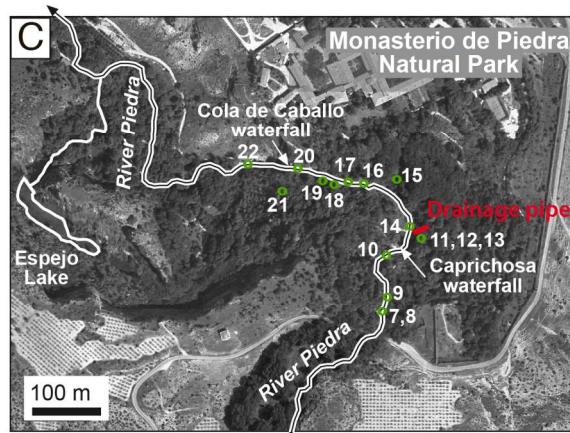
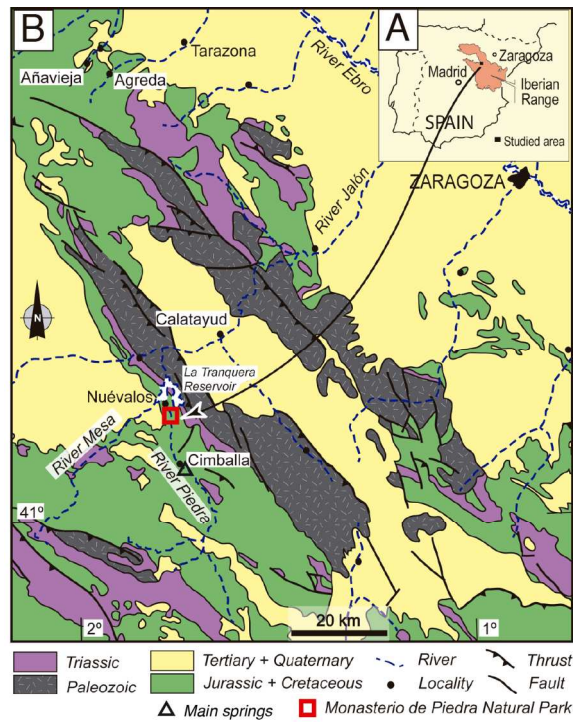
Tw1: Spring + Summer and Autumn+Winter

Tw2: Spring + Summer and Autumn

Measured Tw = Mean of hourly measurements

Cool $\delta^{18}\text{O}_{\text{water}}$ = -8.6 ‰ V-SMOW

Warm $\delta^{18}\text{O}_{\text{water}}$ = -8.5 ‰ V-SMOW



● 14 Studied sites with tablets

